Control and modulation for loss minimization for dc/dc converters in wind farm

Dincan, Catalin Gabriel; Kjær, Philip Carne

Published in:
Proceedings of PCIM Europe 2016 International Exhibition and Conference for Power Electronics, Intelligent Motion, Renewable Energy and Energy Management

Publication date:
2016

Document Version
Early version, also known as pre-print

Control and modulation for loss minimization for dc/dc converter in wind farm

Catalin Dincan, Department of Energy Technology, Aalborg University, cgd@et.aau.dk
Philip Kjær, Department of Energy Technology, Aalborg University, pck@et.aau.dk

Topic Number:10.1; Topic Name: New and Renewable Energy Systems; Wind Farms.
Preferred Presentation Form: Poster Presentation

Abstract

For a DC wind turbine, a single phase series-resonant converter for unidirectional power is studied. This paper aims to identify and compare impact on electrical losses and component ratings from the choice of three candidate control strategies. The evaluation is purely based on circuit simulations and offline post-processing of losses. The initial findings indicate that lower losses are obtained in discontinuous current mode (DCM) conditions, with drawbacks on transformer design.

Series Resonant Converter

HVDC offshore wind farms with MVDC collection grid (Fig.1) promise an increase in efficiency and a reduced bill of materials [1]. One of the key components is the DC/DC converter used in the wind turbine. The proposed DC/DC topology in this paper is a unidirectional series resonant converter (SRC), composed of: inverter, resonant tank, monolithic transformer and medium voltage (MV) rectifier built with series connected diodes. The concept is illustrated in Fig.2 and design specifications are in Table 1.

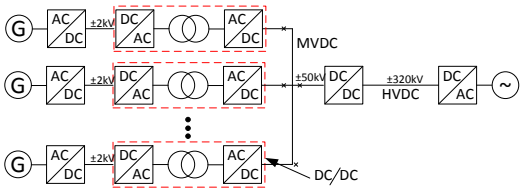

Fig. 1 DC Wind farm diagram

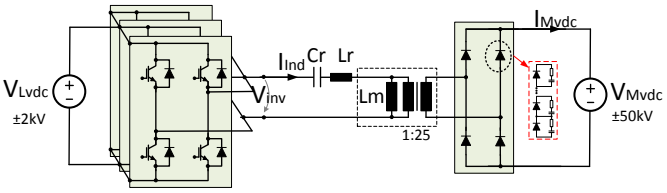

Fig. 2 Converter circuit

Despite the SRC's limitations in control range, it offers an attractive trade-off between component cost (ratings) and electrical losses. Principal advantages are ZCS at turn-off for LV and MV devices, transformer sinusoidal currents and reduced content of harmonics. Bidirectional single phase topology was reported in [2] for railway applications and in [3] a three phase topology was introduced.

Nominal Power	P_n	10 MVA	DC/AC Device	3x4 x IGBT (6500V x 750A)**[4]**
Input DC Voltage	V_{LVDC}	±2 kV	AC/DC Device	4x40 x Diode (6500V x 750A)**[4]**
Output DC Voltage	V_{MVDC}	±50 kV	Isolation level	150 kV
Resonant Capacitor	C_R	78 uF	$I_{Short\_circuit\_MVDC}$	50 x I_{MVDC}
Resonant Inductor	L_R	250 uH	E_{cap}	2500 J
Magnetizing Inductor	L_m	20 mH	E_{ind}	2500 J

Table 1 Converter Nominal Specifications

Problem formulation

The goal of this paper is to apply a methodology which evaluates the impact of different control strategies and modes of operation on losses, stress and component ratings. The evaluation is based purely on circuit simulations.

Methodology

The overall system (control and model of the converter) are performed by using a circuit simulator [5]. The SRC is modelled to estimate the current flow through the devices. It uses ideal switches; stray inductance, capacitance and dead time are not included. Analytical expressions are used to build the semiconductors loss model, while transformer losses are calculated in offline post processor. Finally a comparison of efficiencies and component ratings for different control methods is achieved and ranking of most stress components is performed. These results will impact the resonant converter specifications and design drivers.

Control methods

Three different control methods are discussed: frequency control [6], phase shift [7] and the dual control [8]. Other methods are discussed in [9]. By frequency control of input voltage, the resonant tank impedance is changed. The phase shift method is controlling applied voltage to the resonant tank by changing the duty cycle of the square wave, while having constant excitation frequency. The third method is achieved by combining the two previous methods, being able to control output voltage and the switching current. In [8] phase shift control is implemented on a single phase, bidirectional topology. In [2], the half cycle discontinuous mode series resonant converter (HC-DCM-SRC) is analyzed for traction application.. On the other hand, in [3] a three phase topology was introduced, claiming that frequency control in resonant and super resonant conditions offer highest efficiency.

Modes of operation

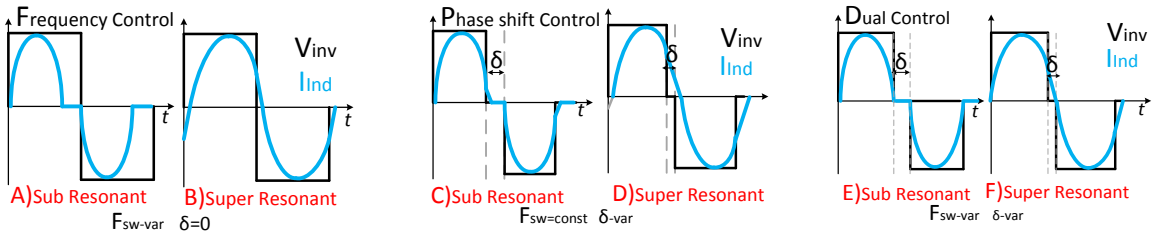

Fig. 3 Modes of operation

For each control strategy, two modes of operation are investigated: sub-resonant and super-resonant (Fig. 3). For sub-resonant, only DCM is considered. In sub-resonant mode, tank current leads applied inverter voltage (Fig. 3 *A,C,E*), while in super resonance it lags (Fig.3 *B,D,F*). In sub-resonant mode, ZCS is possible at turn off, while in super-resonant mode, ZVS is present at turn on. Phase shift control allows passives design at constant frequency, while in frequency control, they have to be designed for lowest switching frequency. Dual control claims to reduce losses compared to phase shift in the entire operational range. No former publication comparing SRC losses with these control strategies and two modes of operation has been identified. The goal of this paper is to fill the gap.

Converter controller

Controller structure is shown in Fig. 4. As the turbine's generator rectifier maximizes the wind energy extraction, the dc/dc converter controls the dc-link voltage. Changes in captured wind power disturb the dc-link voltage, in turn requiring changes to the dc/dc converter power transfer. In the case of sub-resonant frequency control, output power is dependent on the amount of energy transferred to the MVDC link. For a given frequency and duty cycle, output power is a function of number of energy pulses transferred to the output. DC link voltage control is achieved by transferring a certain integral number of pulses to the output. In this case two controllers are used. P_{ref} comes from the dc/dc converter's own dc-link voltage controller and when divided by the measured V_{MVDC}, provides the current reference I_{MVDC}. This current is the output state variable, which is measured and averaged. The feedforward controller equation is determined by the mode of operation, while the PI feedback controller complements the feed-forward controller by correcting its inaccuracies. For frequency control, the output control signal for modulator block is frequency, while for phase shift, it is duty cycle. In case of dual control, both frequency and duty cycle are control variables.

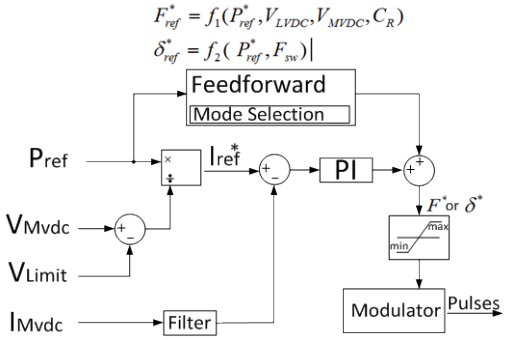

Fig. 4 Controller structure

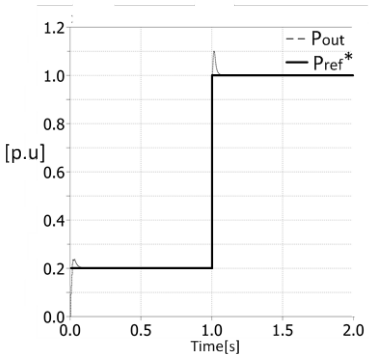

Fig. 5 Output power step response

Fig. 5 shows the output power step response for frequency control, operating in sub-resonant mode. Further on, in Fig.6 and Fig.7, the function of output power to frequency and duty cycle is presented. Two phenomena related to frequency control are noteworthy: as the converter is designed to operate in discontinuous mode in sub-resonance, output power can easily be controlled by frequency in a linear mode. On the other hand, in sub resonance mode, the frequency range is from 1160 to 1200Hz for operation between 1 pu and 0.2 pu output power, and it's not a linear characteristic. Fig.7 indicates that output power can indeed be controlled at constant frequency, by changing the duty cycle of the applied inverter voltage, but in a very limited range. Considering that a change in duty cycle from 0 to 0.225% changes output power from 1 to 0.2pu, the sensitivity of the modulator's impact on output power is a challenge.

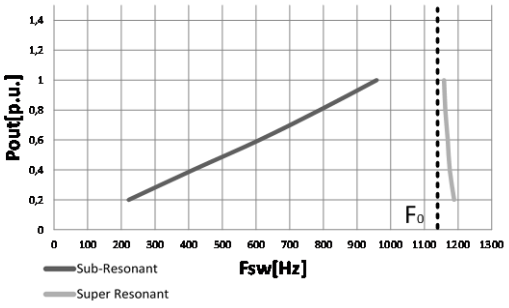

Fig. 6 Pout = f(Fsw)

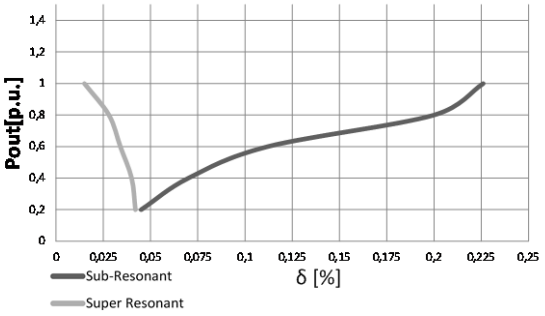

Fig. 7 Pout = f(δ)

Transformer design

The transformer is expected to be the key component in determining the circuit losses. As no standard component is available for the application in mind, dimensions for a preliminary design were used as input to a simplified calculation of transformer losses. Design methodology is similar to [10],[11] and [12]. Only one transformer is used in this converter, with a single primary and a single secondary winding. As no validation has yet been performed in laboratory and to reduce loss model errors, identical transformer designs are proposed for all three modes of operation analyzed. In this manner the same active material is employed. Final transformer specifications are listed in Table 2.

A standard C-core structure, based on amorphous material is pre-selected, with the maximum available size of [13]. In Fig. 8 the winding arrangement is shown. Each leg has a LV and HV winding. Copper foils are used for both. The LV winding is built with a layered construction of *Np* turns, while HV winding has a structure consisting of 37 layers and 25 turns.

The insulation level is set to 150kVAC. NOMEX paper is proposed for windings insulation and mineral oil as main insulation material and coolant. Voltage level and insulator dielectric strength determines minimum distance between primary and secondary *Dins*. According to [11], the insulation level is calculated with:

$$D_{ins} = \frac{V_{ins}}{\lambda \cdot E_{ins}} \tag{1}$$

where E_{ins} is the dielectric strength of the isolation material (in this case oil and paper) and λ is used as a safe margin parameter. In this paper, dielectric losses are neglected, but it needs to be mentioned that increasing the operating frequency and the insulation requirements, the losses can not be neglected in the actual prototype.

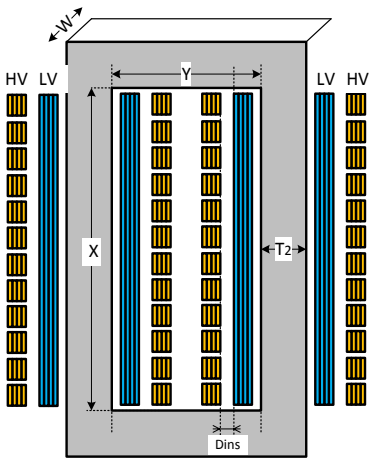

Fig. 8 Transformer drawing

Np (Primary turns)	37 (37 layers x 1 Turn),foil
Ns (Secondary turns)	925 (37 layers x 25 Turns),foil
X (Window height)	1 m
Y (Window width	0.2240 m
T2 (core build)	0.160 m
W(ribbon width)	0.213 m
Core material	Amorphous [13]
Weight of core material	820 kg
Weight of windings	750 kg
Dins	0.0250 m
Bsat	1.63 T
Isolation level	150 kV
Oil dielectric strength	10 kV/mm

Table 2 Transformer specifications

Loss Model

Semiconductors and transformer loss models are presented in Fig. 9 and Fig. 10.

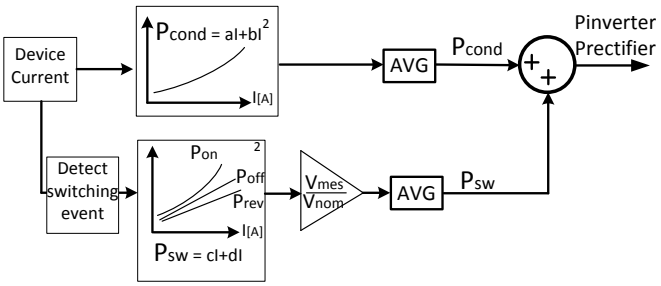

Fig. 9 IGBT and Diode loss model

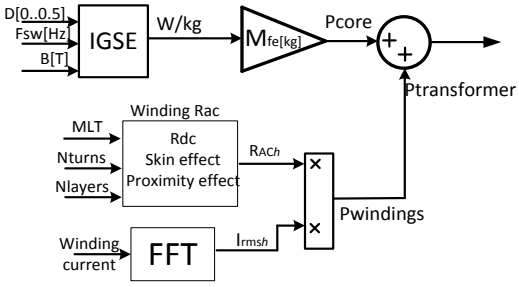

Fig. 10 Transformer loss model

Conduction losses

Methodology proposed in [14],[15] is used for conduction loss modeling for both IGBTs and diodes. The current is multiplied with the according voltage directly from the data sheet for the highest acceptable temperature, e.g. *T=125°C* to extract conduction power loss. Afterwards, the curve is approximated with 2nd order polynomial fitting curves and is described in (2), which uses the current through the ideal switch as input and outputs conduction loss of the device during the simulation. The output is averaged for 1 switching cycle.

Switching losses

Switching losses are determined in similar way like in [14],[15]. Current dependent $E_{ON,}$ E_{OFF} and E_{REC} are given in the device datasheet and are considered for a maximum junction temperature of *T=125°C*. This dependency is approximated with a second order polynomial fitting curve described in (3), and multiplied with voltage factor V_{mes}/V_{nom}, where V_{nom} is datasheet parameter and V_{mes}, actual applied voltage. Whenever a switching event occurs, losses are calculated and then averaged for 1 switching cycle.

$$P_{Cond} = a \cdot I + b \cdot I^2 \qquad (3) \qquad\qquad P_{Sw} = c \cdot I + d \cdot I^2 \qquad (4)$$

Core losses

Different methods have been compared in [10],[11],[12],[16] for core losses. In the present loss model, the *Improved Generalized Steinmetz Equation* (IGSE*)* described in [11] was used with K_i, α and β determined from [16].

$$P_{Core} = K_i \cdot 2^{\alpha+\beta} \cdot f^{\alpha} \cdot \hat{B}^{\beta} \cdot D^{1-\alpha}$$

Winding losses

Foil winding losses are calculates, as according to [10],[11]. The expression from (4) is explained in [10]. The overall losses are calculated by summing the effect of every current harmonic. Skin effect losses are frequency dependent, while proximity losses are influenced by the number of layers. *D* is foil thickness, δ is skin depth and *m* is number of layers.

$$P_{Winding} = R_{DC} \cdot \frac{D}{\delta}\left[\frac{\sinh\left(\frac{D}{\delta}\right)+\sin\left(\frac{D}{\delta}\right)}{\cosh\left(\frac{D}{\delta}\right)-\cos\left(\frac{D}{\delta}\right)} + \frac{2\cdot(m^2-1)}{3}\frac{\sinh\left(\frac{D}{\delta}\right)-\sin\left(\frac{D}{\delta}\right)}{\cosh\left(\frac{D}{\delta}\right)+\cos\left(\frac{D}{\delta}\right)}\right]\cdot I_{rms}^2 \qquad (5)$$

Results

Comparison of losses for the SRC, operated with three different control strategies (frequency, phase shift and dual control) and two modes of operation (sub-resonant and super resonant) are illustrated in Fig. 11 and Fig. 12, for 1pu and 0.5pu output power. First remark in both figures is that transformer core and rectifier losses are similar in all cases, while inverter and winding losses are smaller with frequency control strategy and sub resonant mode.

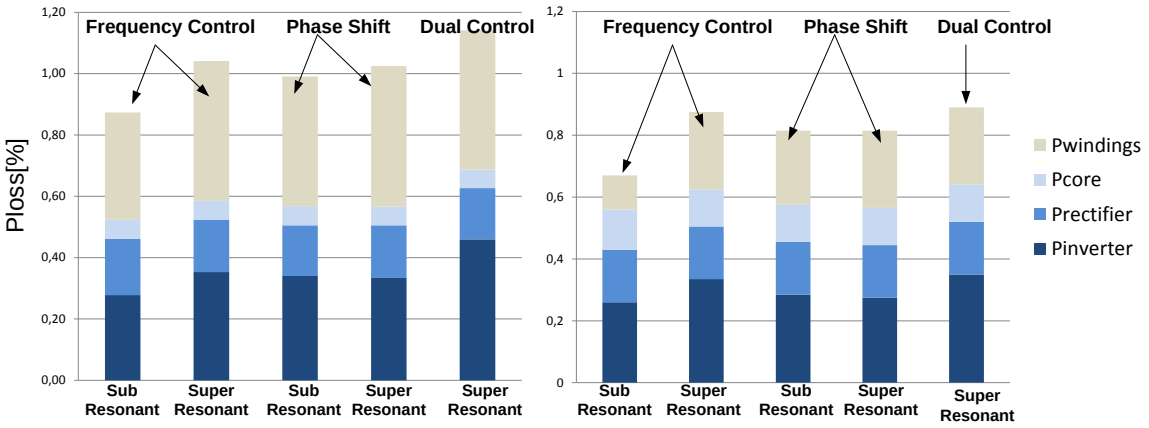

Fig. 11 Losses at 1pu output power

Fig. 12 Losses at 0.5pu output power

Resonant tank stress was evaluated at 1pu output power. Peak inductor current and capacitor voltage are presented in Fig. 13. Highest stress level is present in frequency control-sub resonant, regardless of output power, while for the rest is load dependent. Peak tank energy is show in Fig. 14.

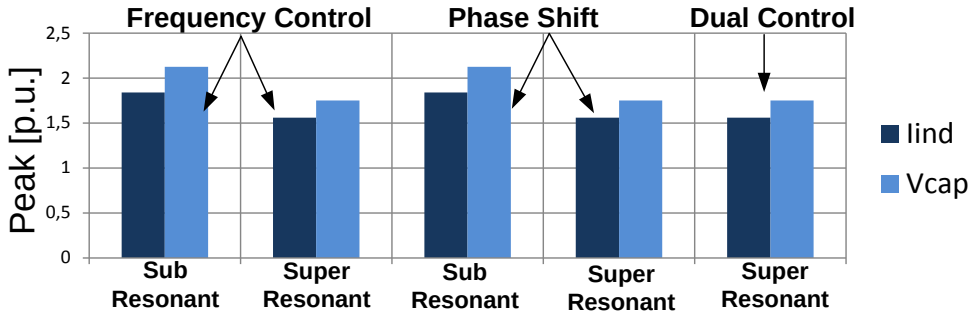

Fig. 13 Inductor current and capacitor voltage pu

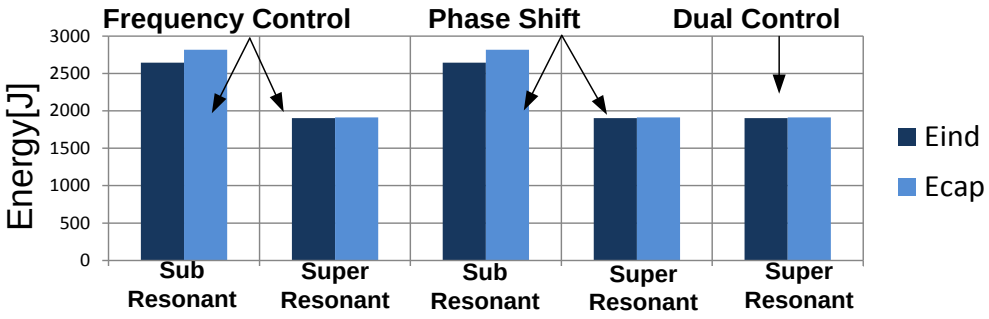

Fig. 14 Inductor and capacitor energy [J]

Discussions

The results in Figures 11 and 12 are now discussed. Firstly, the following were neglected in the loss analysis: (i) Rectifier snubber and resonant tank losses; (ii) ZCS at turn-off has been assumed ideal (truly zero), yet [2] has shown the turn-off losses are not negligible. Planned future characterization of the chosen semiconductors will allow extraction of soft-switching parameters τ and k_s for better loss modelling; (iii) the dual control strategy running in sub-resonance mode is not added to the comparison, as the strategy limits operation above 0.5pu output power. For the SRC, windings losses will be predominant, as they are linear with the squared rms current; therefore transformer characterization is necessary to decrease uncertainties on the windings loss model.

Lowest total losses are found in frequency control sub-resonant mode (0.85%), while the highest total losses occur with dual control in super-resonant mode (1.14%), both at 1pu output power. The difference in simulated losses between all modes is relatively small and is subjective to errors in the loss model, the highest uncertainty being the winding loss model. According to [17], windings loss model is overestimated with ≈15% error. Losses in frequency control sub resonant mode appear smaller, due to small turn on current, while at turn-off they are zero. In super-resonant mode, for all control strategies, ZVS appears at turn on, but turn off losses are considerably higher and winding losses are increased due to higher ac resistance. At elevated frequency, skin and proximity effects increase the winding ac resistance. A strong limitation of frequency control-sub resonant mode is the influence on transformer design, which needs to be designed for the lowest operating frequency. [18] States that no voltage is applied to the transformer during the discontinuous subintervals below 0.5p.u operation. This is true, if the ratio input voltage/output reflected voltage is 2. In current design, the ratio is 1 and it is able to operate in the range from 500Hz and above, as seen in Fig. 16.

Phase shift control can allow designing the transformer for a constant frequency, but the narrow range of duty cycle to output power function will bring sensitivity issues and very low variations in the duty cycle could trigger high power fluctuations. The authors have not yet studied to which degree this sensitivity can be managed in practice. On the other hand, phase shift control does offer an extension to the operational range of frequency control in sub resonant and super resonant mode. Below 0.5pu, phase shift control could be applied, as seen in Fig. 15. Regarding resonant tank stress, in both modes, the tank should be designed for peak values of voltage and current. The peak value is constant in sub-resonant mode (2pu for capacitor voltage and 1.8p. for inductor current) and load dependent in super-resonant mode (1.7pu for capacitor voltage and 1.5pu for inductor current). Peak values will determine selection of semiconductors and number of parallel inverters.

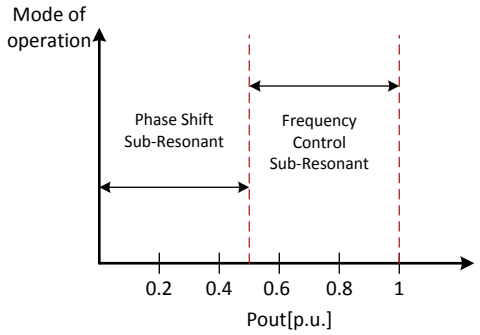

Fig. 15 Range increase in sub-resonant

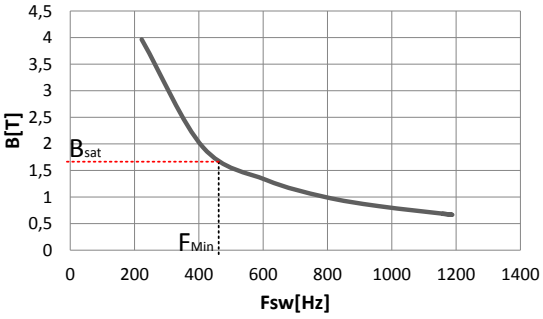

Fig. 16 B_{pk} =f(Fsw)

Conclusions

A single phase, monolithic and unidirectional series resonant converter has been studied for applications in DC wind turbines. A methodology of evaluating the impact of three different control strategies (frequency, phase shift, dual control) on losses and stress has been applied. Semiconductors losses and tank stress were investigated with circuit simulator, while transformer losses calculated in off-line post processor. Frequency control operated in sub-resonance mode has the potential of minimum losses (0.85% in our study, some 10%-25% lower than the compared control strategies) while paying the price of designing the transformer for the lowest operating frequency, which will yield a bulkier design. Tank stress is around 20% higher in frequency control sub-resonant mode, compared to the other strategies and modes. Phase shift and dual control strategies have a narrow control range and could generate high power fluctuations for this particular design. The difference of losses between all modes is small and subjective to loss model error. The highest uncertainty is the windings loss model, which are predominant.

References

[1] C. Meyer, Key Components for Future Offshore DC Grids. 2007.

[2] G. Ortiz, H. Uemura, D. Bortis, S. Member, J. W. Kolar, and O. Apeldoorn, “Modeling of Soft-Switching Losses of IGBTs in DC / DC Converters,”

[3] J. Jacobs, A. Averberg, and R. De Doncker, “A novel three phase series resonant converter for high power Applications,” 2004.

[4] “www.infineon.com.”

[5] “www.plexim.com.” .

[6] R.L.Steigerwald, “A comparison of Hald Bridge Resonant Converter Topologies,”

[7] M. Nakaoka, S. Nagai, Y. J. Kim, Y. Ogino, and Y. Murakami, “The state-of-the-art phase-shifted ZVS-PWM series and parallel resonant DC-DC power converters using internal parasitic circuit components and new digital control,”

[8] P. Ranstad, H. H.-P. H. Nee, and J. Linner, “A novel control strategy applied to the series loaded resonant converter,” 2005 Eur. Conf. Power Electron. Appl., pp. 1–10, 2005.

[9] R. Oruganti and F. C. Lee, “Resonant power processors. II - Methods of control,” vol. I, no. 6, pp. 1461–1471, 1984.

[10] I. Villar, A. Garcia-Bediaga, U. Viscarret, I. Etxeberria-Otadui, and A. Rufer, “Proposal and validation of medium-frequency power transformer design methodology,” [11] G. Ortiz, J. Biela, and J. W. Kolar, “Optimized design of medium frequency transformers with high isolation requirements,”

[12] M. a Bahmani and T. Thiringer, “Design Methodology and Optimization of a Medium Frequency Transformer for High Power DC-DC Applications,”

[13] “http://www.hitachi-hqt.cn/en/core/index.html.”

[14] J. W. Kolar, “A General Scheme for Calculating Switching- and Conduction-Losses of Power Semiconductors in Numerical Circuit Simulations of Power Electronic Systems.”

[15] K. Lee, Y. Suh, and Y. Kang, “Loss Analysis and Comparison of High Power Semiconductor Devices in 5MW PMSG MV Wind Turbine Systems,”

[16] R. U. Lenke and R. U. Lenke, E . ON Energy Research Center A CONTRIBUTION TO THE DESIGN OF ISOLATED DC-DC CONVERTERS FOR UTILITY APPLICATIONS A Contribution to the Design of Isolated DC-DC Converters for Utility Applications. .

[17] I. Villar, U. Viscarret, I. Etxeberria-Otadui, and A. Rufer, “Global loss evaluation methods for nonsinusoidally fed medium-frequency power transformers,”

[18] R. W. Erickson, Fundamentals of Power Electronics, Second edition. .